Physica Medica 136 (2025) 105032

Contents lists available at ScienceDirect

Physica Medica

journal homepage: www.elsevier.com/locate/ejmp

Original paper

Rapid and reversible adaptation of a clinical linear accelerator for electron FLASH radiotherapy

Frank Schneider [a], Cornelius J. Bauer [a], Ida D. Göbel [a], Clarence King [b,c,d], Maria Francesca Spadea [b], Joao Seco [c], Frank A. Giordano [a,e,f], Jens Fleckenstein [a,*]

[a] Department of Radiation Oncology, University Medical Centre Mannheim, University of Heidelberg, Germany
[b] Institute of Biomedical Engineering, Karlsruhe Institute of Technology (KIT), 76131 Karlsruhe, Germany
[c] Division of Biomedical Physics in Radiation Oncology, German Cancer Research Center (DKFZ), Heidelberg 69120, Germany
[d] Department of Physics and Astronomy, Heidelberg University, Heidelberg 69120, Germany
[e] DKFZ-Hector Cancer Institute, University Medical Centre Mannheim, Mannheim, Germany
[f] Mannheim Institute for Intelligent Systems in Medicine (MIiSM), Medical Faculty Mannheim, University of Heidelberg, Mannheim, Germany

ARTICLE INFO

Keywords:
FLASH
Ultra-high dose rate
LINAC
Dosimetry
Electron beam

ABSTRACT

Purpose: The aim of this work was to establish a procedure that allows the conversion of a standard clinical LINAC into a "FLASH" LINAC capable of delivering ultra-high dose rates above 40 Gy/s, with minimal, fully reversible modifications to the device. A dosimetric characterization of the resulting treatment beam is presented.
Methods: A LINAC was modified to emit a 10 MeV electron FLASH beam. Modifications included the integration of a pulse control unit which consisted out of a scintillation detector and a transistor circuit. Beam parameters were optimized to maximize dose output. Beam characterization measurements were performed with different detectors in water: ionization chamber, diamond detector, radiographic films and scintillation detector. The resulting doses per pulse (DPP) and dose rates at different source-surface-distances (SSD) as well as the output reproducibility were determined. The beam was characterized with depth dose curves and lateral profiles.
Results: Conversion of a LINAC to FLASH mode was feasible in less than 30 min. Output was between $DPP_{SSD=56cm} = 1.69 \pm 0.02$ Gy and $DPP_{SSD=100cm} = 0.53 \pm 0.01$ Gy or dose rates between 676 ± 8 Gy/s and 213 ± 4 Gy/s. Reproducibility of DPP was better than 0.8 %. FLASH depth dose curves showed a higher range (R80 = 39.8 mm vs. 34.6 mm) and lateral beam profiles had a reduced flatness (from 5.5 % to 12.7 %) at SSD = 56 cm.
Conclusion: We present a fully reversible conversion method requiring minimal modifications to a LINAC to produce electron FLASH beams. The achieved DPP and mean dose rates demonstrated high reproducibility, meeting criteria for FLASH applications, and markedly simplifying access to this technology for broader implementation.

1. Introduction

Ultra-high dose rate (UHDR) FLASH radiation therapy (UHDR > 40 Gy/s) has attracted considerable attention in the radiotherapy community for its promise to reduce normal tissue toxicity while maintaining adequate tumor control. In order to fully explore its therapeutic potential, both appropriate dosimetry and preclinical research with cell experiments to better understand the radiobiological mechanisms [1] and with small animals to demonstrate the therapeutic effect of FLASH [2] are currently being investigated. In addition, the first human clinical trials are underway (IMPULSE, LANCE, FAST-01, FAST-02) [3].

Several different technical realizations of ultrahigh dose rates are used [4]: dedicated research facilities, modified clinical facilities or dedicated treatment units for clinical FLASH treatments [3]. Currently, almost all preclinical and clinical studies are therefore performed with either electrons, protons or heavy ions in their respective conventional therapeutic energy ranges. The introduction of FLASH with very high energy electrons (VHEE) [5] or photons [6] is currently under development. While most proton [7,8] or heavy ion [9] therapy machines are modified clinical beamlines that can be used in FLASH and conventional

* Corresponding author at: Department of Radiation Oncology, University Medical Center Mannheim, Heidelberg University, Theodor-Kutzer-Ufer 1-3, 68167 Mannheim, Germany.
E-mail address: Jens.Fleckenstein@medma.uni-heidelberg.de (J. Fleckenstein).

https://doi.org/10.1016/j.ejmp.2025.105032
Received 12 April 2025; Received in revised form 28 May 2025; Accepted 20 June 2025
Available online 23 June 2025

(CONV) radiotherapy modes, there are few conventional medical linear accelerators (LINACs) that can be operated in CONV and FLASH modes without beamline adjustments and with minimal modifications.

In the context of electron FLASH, several research groups report the modification of a LINAC for FLASH purposes, either by removing the LINAC treatment head [10] or by modifying the clinical LINAC beamline to achieve FLASH dose rates. Table 1 gives an overview of the different LINAC modifications together with the most relevant electron beam FLASH parameters: the electron beam energy, the dose rate at the isocenter (ISO), the dose per pulse (DPP) and the pulse repetition frequency (PRF). Together with the corresponding pulse width (Elekta LINACs 3.3 μs [10] and Varian LINACs 4.2 μs [11]) the instantaneous dose rate can be determined.

In this work, we present a modification of a LINAC that allows for alternating between patient treatment mode with conventional beams and FLASH research mode with a 10 MeV beam quality with minimal fully reversible modifications to the clinical LINAC and a short modification time. Furthermore, a dosimetric characterization of the resulting FLASH beam is performed.

2. Materials & methods

2.1. Pulse control system

An external system was designed to control the pulse delivery. To detect individual radiation pulses emitted from the LINAC we utilized a plastic scintillation detector (SD) (model 11.0, BluePhysics, Tampa, FL, USA) [20] with an active volume of 0.8 mm^3 and time resolution of 625 μs, attached to an electrometer and dedicated software (BlueSoft, v. 11.1). At a PRF of maximum 400 Hz (2.5 ms/pulse), this enables detection of individual pulses. The acquisition unit features a 5 V output signal, which can be used as a trigger for third-party devices. This output signal was sent to a transistor circuit consisting of a MOSFET (IRLD014, SiHLD014, Vishay Siliconix), a 10 kΩ pull-down resistor, and a 1 kΩ resistor to limit the MOSFET current. The transistor circuit functions as a fast switch to control the PRF interlock (see section 2.2). The pulse control workflow is summarized as follows: The radiation is activated using the function keypad of the LINAC. By default, the acquisition unit outputs a 0 V signal to the transistor circuit, thereby interrupting the PRF interlock signal of the LINAC ("PRF En. Chk inhibit" status). Upon pressing start in BlueSoft, the acquisition unit outputs a 5 V signal to the transistor circuit, thereby closing the PRF interlock signal. Consequently, the LINAC starts to deliver radiation. The radiation pulses are detected by the SD, which is mounted to the Mylar crosswire sheet and are counted in the software. After detecting a predefined number of pulses, the acquisition unit once again outputs a 0 V signal to the transistor circuit, interrupting the PRF interlock signal. A schematic drawing of the pulse-control circuit is displayed in Fig. 1.

Table 1
Overview over previously performed LINAC conversions to FLASH mode with their key parameters. Treatment distance was mostly not at ISO, but is reported here for the sake of comparability. LINAC type, electron energy, dose rate and dose per pulse (DPP) at ISO as well as pulse repetition frequency (PRF) are displayed.

Research group	LINAC	Electron energy [MeV]	Dose rate @ ISO [Gy/s]	DPP @ ISO [Gy]	PRF [Hz]
Schuler et al.[12]	Varian Clinac 21EX	9, 20	<25		180
Konradsson et al. [13,14]	Elekta Precise	10	>200	1.1	200
No et al. [15]	Varian Trilogy	16	36.8		
Rahmann et al. [16]	Varian 21EX	10	290	0.8	360
DalBello et al. [11]	Varian TrueBeam	16	256	1.3	200
Cetnar et al. [17]	Varian Clinac iX	16	197	1.1	180
Sloop et al. [18]	Varian 21EX Varian Trilogy	10	432	1.2	360
Deut et al. [19]	Elekta SL	10	83.6	0.6	100

2.2. LINAC modifications

A medical linear accelerator (Synergy, SN 152092, Elekta AB, Stockholm, Sweden) was modified according to the methodology described by Lempart et al. [14] to facilitate the delivery electrons at UHDR. In order to be able to rapidly alternate between clinical operation and UHDR research applications, the software and hardware modifications were minimized and designed to be fully reversible.

2.2.1. LINAC software modifications

In service mode, a new "electron energy" (Elekta energy calibration) was defined and labeled as "FLASH". This energy calibration is accessible exclusively in the LINAC's service mode and can independently be adjusted without affecting clinical electron energy settings. For the UHDR electron energy calibration, we used the magnetron parameters (charge rate and magnetron magnet), electron gun parameters, and bending section settings of a default 10 MV X-ray beam, which were adjusted by an Elekta service engineer. Further dose rate optimization was achieved by fine-tuning the electron gun and high-frequency parameters (see section 2.3). All possible scatter material within the beam was minimized: the target block was moved to the electron window, the primary filter assembly was moved to the open electron port and an unused and empty port of the secondary filter was selected. Additionally, the backscatter plate (shutter) was moved out of the beam (default electron configuration). As a result, only the electron window, the ionization chamber, the mirror for the optical system and the Mylar crosswire sheet remained within the beam.

2.2.2. LINAC hardware modifications

The unused port of the secondary filter was originally covered with a lid, which was permanently removed. Since this port is not utilized for clinical electron energies, its removal does not impact clinical operations. The LINAC's PRF interlock was used to control beam interruption, utilizing the same approach that is used for clinical gating via the LINAC's response interface. One of the PRF interlock breakout points is located in area 12 of the LINAC, where we inserted an adapter cable between the plug and socket, bridging all signal pins except the PRF interlock. This allowed for the integration of the pulse control system.

The FLASH beam is expected to produce a high electrical current in LINAC's ionization chamber. Thus, to prohibit potential damage of the electronics, we disconnected the ionization chamber signal and voltage cables in area 12. Instead a second mock-up ionization chamber, which was not positioned within the beam line, was connected to the electronics to avoid LINAC interlocks due to a missing ionization chamber.

2.3. Beam optimization/ dose rate maximization

By default, a PRF of 400 Hz was used. For all optimization steps, the following settings were applied:

a) The gun servo, 2 T, and 2R were set to "manual" to disable automatic beam adjustments.
b) Cascade PRF (Item 602, part 131), was set to zero to prevent a gradual increase in PRF from 25 Hz to 400 Hz over the initial pulses. As a result, a PRF of 400 Hz was achieved from the first pulse onward.
c) Only "Gun I Ctrl" (item 327), "Gun Stby I" (item 380), "Tuner Ctrl" (item 161) and "Tuner Rest" (item 97) were adjusted to maximize the dose output.

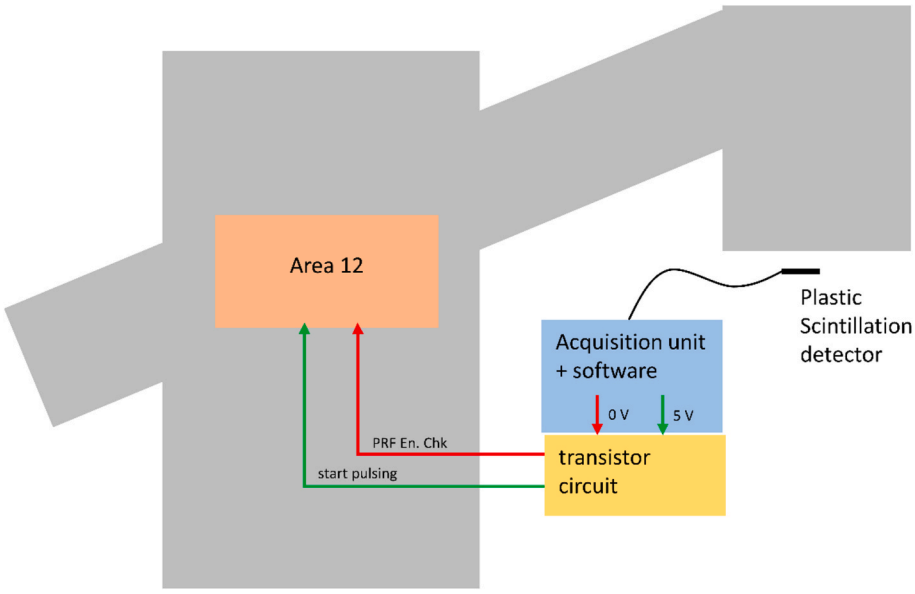

Fig. 1. Schematic drawing of the pulse control system interacting with the LINAC.

2.3.1. Determination of a stable frequency

To identify a stable frequency, we loaded the "FLASH" energy setting while inserting the electron target, as well as the primary and secondary filters (x-ray settings), to prevent UHDR delivery. The tuner was initially set to automatic mode, and "Tuner Rest" (item 97) was incrementally increased in steps of five units, ranging from position 100 to 260. At each step, the beam was activated, and within the first few seconds, we monitored whether "Tuner Ctrl" (item 161) stabilized at a defined value before further increasing due to thermal effects. This approach enabled the identification of three tuner positions with stable frequencies. These operating points were subsequently used to determine a suitable electron gun current.

2.3.2. Optimize gun current

In a second step, the "Gun I Ctrl" (item 327) was incrementally decreased in steps of 0.05 units, ranging from position 7.4 down to 6.5, for each previously identified stable frequency until a measurable output was detected. To minimize thermal effects, the beam was activated only for a few seconds at each step. This optimization process ultimately resulted in a single stable combination of frequency and electron gun current.

2.3.3. Fine tuning

In a third step, we switched to FLASH mode, removed the electron target as well as the primary and secondary filters, set the tuner control to "manual" mode, and connected the pulse control system. A slab phantom setup, equipped with an Advanced Markus ionization chamber (AM)(Type 34045, PTW, Freiburg, Germany), was positioned at a depth of 3 cm and a source-surface-distance SSD = 56 cm. The optimization process began with the magnetron tuner position identified in step two, reduced by five digits, and was then incrementally increased in steps of 0.3. For each step, five pulses were delivered until the maximum dose was measured using the AM. The same procedure was then applied to the "Gun Stby I" (item 380): starting from the value estimated in step two, reduced by 0.2 digits, and incrementally increasing in steps of 0.01 until the maximum dose was identified.

2.3.4. Warm up procedure

In the final step, we evaluated a warm-up procedure for the magnetron, waveguide, and gun to stabilize the beamline, as this typically occurs automatically in clinical mode after a few seconds of beam operation. To preheat the magnetron and waveguide, we set the "Gun Stby I" (item 380) to its minimum value (0.24) and reduced the final "Tuner Ctrl" (item 161) by 40 digits. The system was then operated for a predefined duration before the beam was interrupted, and both "Gun Stby I" and "Tuner Ctrl" were reset to their optimal values. Five pulses were subsequently delivered. The warm-up duration was incrementally increased in 15 s steps, ranging from 0 to 120 s, until the maximum dose was restored.

The SD, controlling the pulses, showed that the first pulse was consistently lower than the subsequent four pulses. To address this issue, an additional gun warm-up procedure was established. Following magnetron warm-up, the "Gun Stby I" and "Tuner Ctrl" was set to its optimal value while keeping the beam interrupted. The gun was then operated for a designated period, after which the five pulses were delivered. The gun warm-up duration was incrementally increased in 15 s steps, ranging from 0 to 90 s. Finally, we repeated the fine-tuning procedure (step three) to determine whether further optimization of dose and related dose rate or DPP could be achieved.

Final workflow:

The procedure to achieve the maximum DPP is summarized in Fig. 2 and was as follows:

a. The beam was initiated with "Gun Stby I" (item 380) set to 0.24 and "Tuner Ctrl" (item 161) set to 170, waiting for the "PRF En. Chk inhibit" status.
b. The start button in BlueSoft was pressed, triggering the delivery of a defined number of pulses. During this phase, the "PRF En. Chk inhibit" status disappeared, and the high-frequency system operated for 75 s to warm up the magnetron and waveguide.
c. The beam was then interrupted, "Gun Stby I" (item 380) was adjusted to 7.1 for gun warm-up, and "Tuner Ctrl" (item 161) was set to 211.5.
d. After a 45 s gun warm-up, the beam was restarted, five pulses were delivered, and again interrupted by the pulse control system.

2.4. Dosimetry

For acceptance and commissioning of electron FLASH units we followed the recommendations of Palmiero et al. [21] (without consideration of different gantry angles). A key-concept of their work is that reference dosimetry for FLASH electron beams should be performed by redundancy. We therefore used four independent dosimetry methods: AM, diamond detector (FD, flashDiamond, TM60025 and flashAdapter

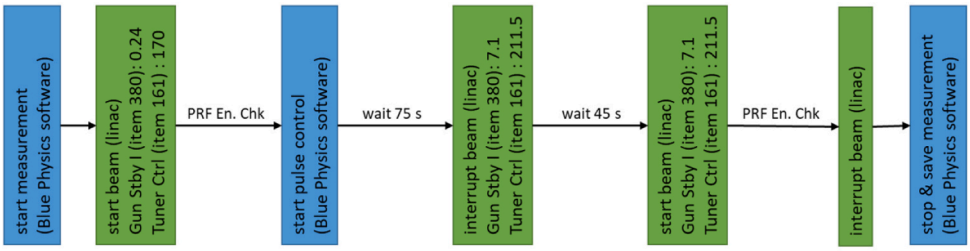

Fig. 2. Optimized workflow to achieve the maximum dose per pulse.

TM16055, PTW, Freiburg, Germany) [22,23], radiochromic films (RF, Gafchromic XD, LOT 05092402, Ashland Inc., Covington, USA) and SD.

2.4.1. Reference phantom setup

An AM, a SD, a FD and RF were mounted on a PMMA platform positioned within a water phantom at source-surface-distance SSD = 56 cm as displayed in Fig. 3a. The water phantom itself was positioned on the LINAC treatment couch. The FD and the SD were oriented perpendicular to the beam axis, with their centers positioned at a depth of 24 mm, 5 mm lateral to the central beam axis. The RF was placed at a depth of 28 mm, while the AM was positioned directly beneath it, with its active volume located at a depth of 29 mm.

A PMMA slab, incorporating an 8×8 cm^2 square lead aperture, was placed on top of the basin at SSD = 54 cm. The UHDR beam was pre-collimated using multi leaf collimator (MLC) and jaws to a field size of 8.1×8.1 cm^2 at SSD = 54 cm.

2.4.2. Ionization chamber dosimetry

The absorbed dose in water measured with AM was determined according to DIN 6800–2 reference dosimetry protocol. Although measurements were not performed under reference conditions, the electron beam quality factor k_E (or k_Q according to IAEA TRS-398 report) corresponding to a standard clinical 10 MeV electron beam was applied. The ionization chamber's charge collection efficiency, k_s, was determined on a per-pulse basis using equation (1) by Petersson et al. [24]

$$k_s = \left(1 + \left(\frac{DPP[mGy]}{k_s \cdot U[V]}\right)^{\gamma}\right)^{\delta}. \quad (1)$$

DPP/k_s was the detector reading in [mGy], U was the applied detector voltage (300 V) and $\gamma = 3.1$ and $\delta = 0.18$ were constants. The polarity factor k_{pol} was defined as 1.

2.4.3. Radiochromic film dosimetry

RF were used for point- and spatial dosimetry. A scanner (Expression 12000XL, Seiko Epson Corporation, Suwa, Japan) was used in transmission mode to digitize the irradiated RF. 48 bit TIFF images with 72 dots per inch resolution were stored. All RF were scanned 24 h after irradiation and calibrated to absolute dose. This color-to-dose-calibration was performed with the 16 bit red channel data R and AM measurements. A 39 point calibration curve in 0.5 Gy increments between 0 and 10 Gy and 1.7 Gy dose increments between 10 and 30 Gy was obtained at conventional 10 MeV electron beams and a dose rate of 4 Gy/min.

To obtain the RF doses D_{RF} out of R a regression with the function

$$D_{RF} = a + \frac{b}{\log(R) - c} \quad (2)$$

was performed. Model parameters were a = -27.01 Gy, b = 55.44 Gy, c = 8.75. The mean absolute relative error was 3.0 %, the root-mean-square-error RMSE = 21.8 cGy, and $R^2 = 0.9994$.

2.4.4. Diamond detector dosimetry

The absorbed dose in the FD was estimated by cross-calibrating it against the AM in a conventional 10 MeV electron beam. For this purpose, the AM was positioned at the reference depth within an RW3 slab phantom (PTW, Freiburg, Germany) and irradiated using reference beam parameters. The electrometer reading was corrected according to DIN 6800–2 protocol. The FD, oriented perpendicular to the beam axis,

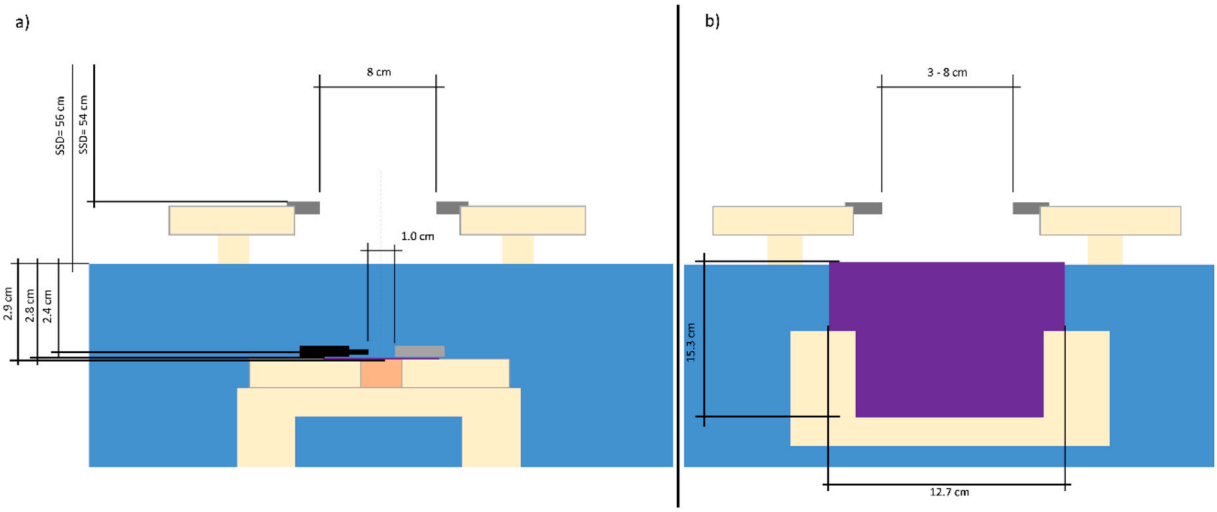

Fig. 3. (a) Reference setup for the dosimetry measurements with the SD (black) and the FD (grey) on top of the RF (purple) on top of the AM (orange). Brown color indicates PMMA while dark grey color represents the lead aperture. (b) The analogue measurement setup for film measurements to evaluate the spatial dose distributions. Two RF (purple) were positioned vertically in a water basin once in IL and once in CL orientation. (For interpretation of the references to color in this figure legend, the reader is referred to the web version of this article.)

was placed with its center at the same depth as the AM. Each measurement was repeated three times. Finally, the mean absorbed dose measured with the AM was divided by the averaged reading from the FD detector to obtain the calibration factor.

2.4.5. Scintillation detector dosimetry

The SD that was used for pulse detection was also used for dosimetry. A calibration to dose D_{SD} was acquired [20] via

$$D_{SD} = CF \times (R_s - ACR \times R_c), \quad (3)$$

Where R_s in [nC] is the detector's sensor signal, R_c in [nC] is the detector's Cherenkov signal, ACR = 91.6 % is the adjacent channel ratio. The calibration factor CF = 36.06 10^{-3} Gy/nC was acquired at FLASH dose rates through cross calibration with the FD. For this purpose, between 1 and 25 pulses were delivered and a linear regression (R^2 = 0.997) between FD and SD was performed.

2.5. FLASH beam characterization

2.5.1. DPP reproducibility

Using the aforementioned phantom setup, we delivered ten irradiations, each consisting of five pulses. All detectors were irradiated simultaneously to assess the reproducibility of both pulse delivery and detector readings. DPP for each detector was evaluated. To compare the DPP at SSD = 56 cm with DPP at ISO an additional measurement using the same phantom setup was performed at SSD = 100 cm.

To assess the reproducibility of the pulses, the same measurement was repeated while varying the number of pulses from 1 to 25. For each pulse count, five measurements were performed for AM, FD and SD and three for RF with all detectors simultaneously and DPP was evaluated. To assess the dependence on PRF, measurements of five pulses were repeated at frequencies of 400 Hz, 200 Hz, 100 Hz, 50 Hz, and 25 Hz. In this setup, the AM, FD, and SD were used for dosimetry. Each measurement was repeated five times.

2.5.2. Characterization of the spatial dose distribution

The spatial dose distribution was measured by irradiating a RF in vertical orientation within a water phantom. To estimate uncertainties between individual RF, two RF were taped together and irradiated simultaneously. To prevent movement or tilting, the RFs were secured between two U-shaped plastic frames (Fig. 3b). A PMMA slab, incorporating different lead apertures (circular opening diameters: 2 cm, 3 cm, 4 cm, 5 cm, 7 cm, 8 cm and a square opening of 8x8 cm^2), was placed on top of the phantom. The phantom itself was positioned on the LINAC treatment couch, with the water surface aligned at a SSD = 56 cm. The measurements, each with nine pulses, were repeated in inline (IL) and crossline (CL) orientation for each aperture. Using the squared aperture, the measurement was repeated at SSD = 100 cm with the lead aperture placed in a standard 10 × 10 cm^2 electron applicator, as well as with conventional 10 MeV electron beams at SSD = 56 cm. For these radiation fields, flatness was evaluated according to AAPM TG45 definition. All calibrated RF were aligned in myQA (IBA Dosimetry, Schwarzenbruck, Germany). To evaluate the depth dose curve, the four RF of each aperture were averaged and the central axis was extracted. Finally, the two crossline RF were averaged to assess the lateral profiles.

3. Results

Time to convert a clinical LINAC into FLASH mode (without any further beam optimization) was less than 30 min. With optimized settings but without warmup procedure a reduced reproducibility with $DPP_{SSD56cm} = 0.7Gy - 1.0Gy$ was detected. After, applying the warmup procedure, a $DPP_{SSD56cm} = 1.69 \pm 0.02Gy$ or a dose rate of $\dot{D}_{SSD56cm} = 676 \pm 8Gy/s$ averaged over all detectors and pulse deliveries was achieved at SSD = 56 cm. In analogy, a $DPP_{SSD100cm} = 0.53 \pm 0.01Gy$ and a dose rate $\dot{D}_{SSD100cm} = 213 \pm 4Gy/s$ was found at SSD = 100 cm. The DPP and its reproducibility of 10 consecutive 5-pulse dose deliveries measured with the four different detectors are shown in Table 2.

The DPP as a function of the number of delivered pulses is displayed in Fig. 4a. The average relative standard deviation for all measurements with a certain detector was 0.8 % for AM, 0.8 % for FD, 2.0 % for SD and 3.9 % for RF.

The DPP as a function of the PRF for a five pulse delivery is displayed in Fig. 4b. All detectors revealed a moderate decrease (9.0 % reduction at 25 Hz) in DPP when the PRF was reduced. In Fig. 4c-d the corresponding relative measurement uncertainties (one standard deviation) are presented. It can be seen that the uncertainties in AM and FD measurements change similar to each other with varying pulse numbers. Since measurements were performed with all detectors simultaneously during one dose delivery, this behavior can be attributed to a dose delivery uncertainty ($\sigma < 0.8$ %) rather than a measurement uncertainty. Furthermore, a decrease of the uncertainty with an increase in the number of delivered pulses was not observed. This would be the case if uncertainty on a pulse-by-pulse level existed.

The central axis depth dose curves for different circular apertures are shown in Fig. 5a. It can be observed that for apertures smaller than 5 cm, the dose maximum (d_{max}) shifts closer to the water surface. While d_{max} is located at 29 mm for apertures of 5, 7, and 8 cm, it decreases to 24.0 mm, 21.5 mm, and 15.5 mm for 4 cm, 3 cm, and 2 cm apertures, respectively. The percentage depth dose (PDD) curve of beams collimated with the 8 cm squared aperture (Fig. 5b) shows for the different SSD differences predominately before its dose maximum for the FLASH beam. The maximum penetration depth of the FLASH beam, at SSD = 56 cm, is similar to that at SSD = 100 cm. However, by removing the primary and secondary filters the FLASH beam has a less attenuated energy spectrum and therefore a higher residual range in water. The range $R_{80\%}$ of the electron beams were (39.8, 39.5, 34.6) mm for (FLASH SSD = 56 cm, FLASH SSD = 100 cm, CONV SSD = 56 cm). The crossline profiles in d_{max} for all circular apertures are shown in Fig. 5c. It can be seen that with apertures smaller 5 cm the absolute dose decreases due to a lack of lateral scatter. In Fig. 5d normalized CL profiles for FLASH and CONV at a depth of 5 mm are presented. Flatness according to AAPM TG45 definition for (FLASH SSD = 56 cm, FLASH SSD = 100 cm, CONV SSD = 56 cm) was (12.7 %, 6.2 %, 5.5 %). The FLASH beam at SSD = 56 cm shows a non-uniform lateral intensity distribution which has to be expected at this reduced distance to the target and due to the removal of all scatter material in the beam path. The respective CONV beam at the same distance shows a uniform profile. At SSD = 100 cm, however, the FLASH beam is also sufficiently far away from the source to reveal a uniform dose profile.

4. Discussion

Among the presented modifications of conventional LINACs to allow for FLASH, this work followed the approach of a minimum modifications needed to robustly deliver UHDR. Averaged over all detectors, dose rates between 676 Gy/s at the most upstream treatment position outside the LINAC's treatment head at SSD = 56 cm and 213 Gy/s at isocenter were achieved and are comparable to those reported from other research groups (Tab. 1). Dose deliveries were reproducible and dose per pulse was independent of the number of delivered pulses and slightly

Table 2
Dose per pulse (DPP) at SSD = 56 cm and SSD = 100 cm and its standard deviation for 10 repeated 5-pulse dose deliveries measured with different detectors: advanced Markus ionization chamber (AM), flashDiamond (FD), radiochromic film (RF) and scintillation detector (SD).

SSD	DPP(AM) [Gy]	DPP(FD) [Gy]	DPP(RF) [Gy]	DPP(SD) [Gy]
56 cm	1.68 ± 0.02	1.70 ± 0.02	1.74 ± 0.04	1.75 ± 0.04
100 cm	0.53 ± 0.01	0.53 ± 0.01		0.54 ± 0.02

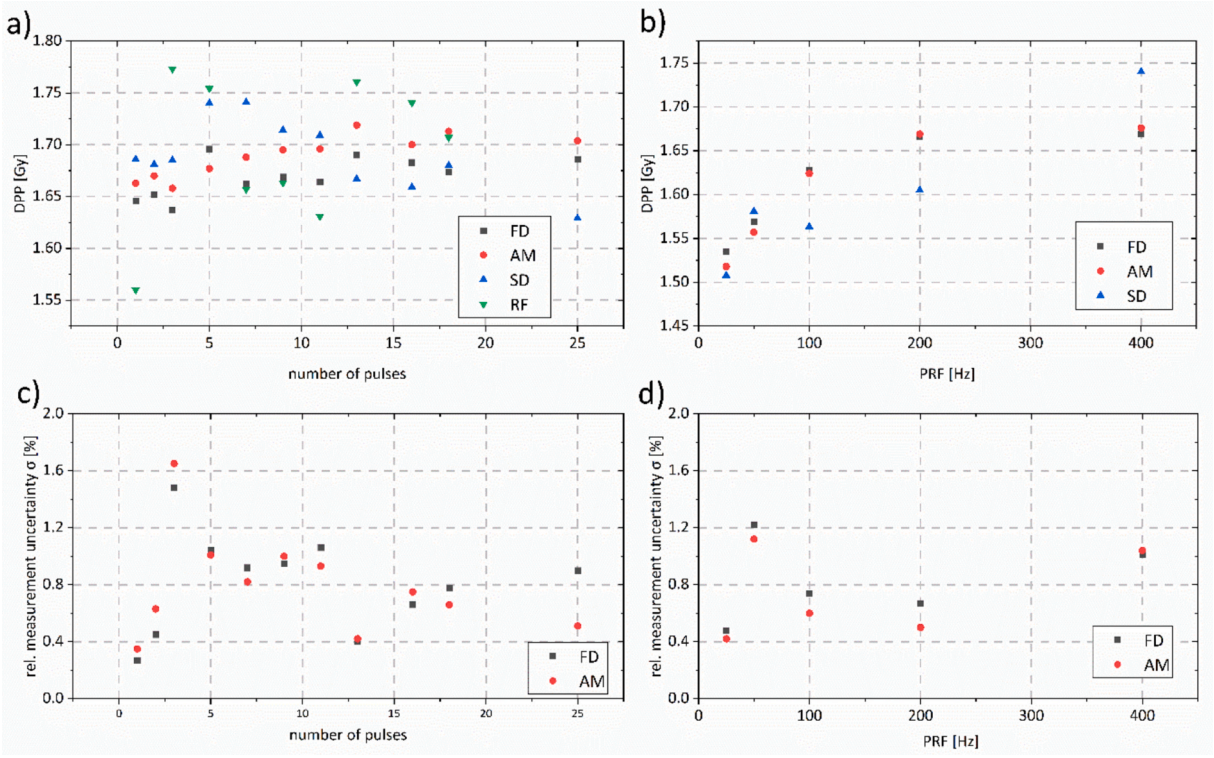

Fig. 4. (a) Dose per pulse (DPP) as a function of number of delivered pulses for four different detectors. (b) DPP as a function of pulse repetition frequency (PRF) for three different detectors. The corresponding relative measurement uncertainties (one standard deviation) for advanced Markus ionization chamber (AM) and flashDiamond (FD) are displayed in panels (c) and (d).

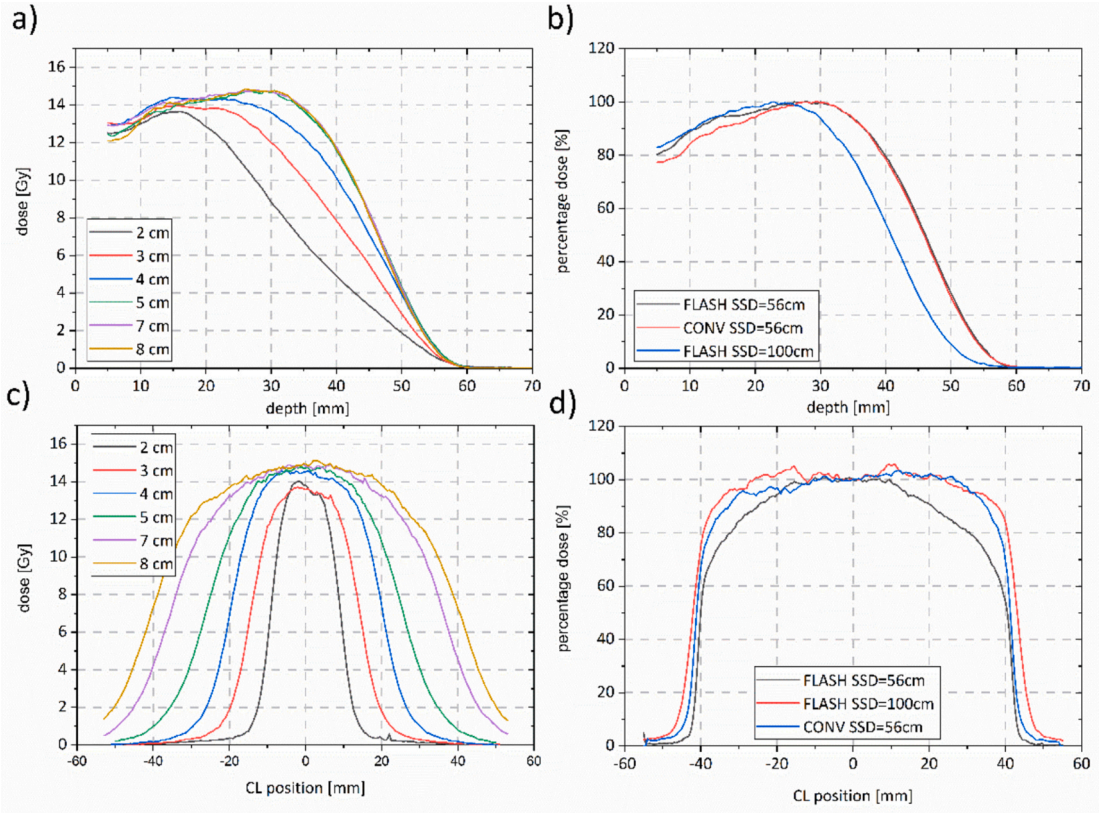

Fig. 5. FLASH central axis depth dose curves (a) and CL-dose-profiles in d_{max} (c) for different circular apertures. All data were acquired at source surface distance SSD = 56 cm. Percentage depth dose curves (b) and CL-profiles in 5 mm depth (d) for FLASH at different SSD and CONV at SSD = 56 cm are displayed.

dependent on the pulse-repetition frequency. A PRF of 400 Hz is, to our knowledge, currently the highest reported. Further fine tuning of the DPP output by e.g. optimizing the magnetron settings [13,18] could increase dose rates even further.

Omission of the relevant filters had two consequences on the shape of the beam: First, the range was increased due to less absorber material within the beam and second, a more pronounced variation of lateral profile shapes with varying SSD was found. At SSD = 100 cm those lateral profile shapes were comparable to the CONV beam.

To perform accurate dosimetry in the FLASH radiation fields, four independent detectors were used: Ionization chamber, FLASH diamond detector, scintillation detector and radiochromic films. For the ionization chamber measurements, the approach of Petersson et al. [24] to use a DPP-dependent correction factor k_s for ion recombination was used. The fact that we used the k_E factor determined under conventional reference conditions for the advanced Markus chamber is a potential source of error, since the electron energy spectrum was clearly different from a conventional 10 MeV electron beam at SSD = 100 cm (Fig. 5b). Rinati et al. [23] demonstrated the dose rate independence of the FD over the relevant range of DPP, which has also been demonstrated for scintillation detectors [17,25]. The FD and AM showed a slight difference of 1.2 %, which may be due to differences in k_E or k_{pol} for the AM or uncertainties in the calibration of the AM or FD. Radiochromic films have been calibrated against an AM at standard dose rates and are also dose rate independent [26–28]. The first 5 mm of the radiochromic films are not shown in Fig. 5a-b because they were prone to image artifacts due to the film cutting process and their exposure to water. In addition, inaccuracies in the lateral profiles in Fig. 5c-d for 2D film dosimetry may be due to the non-uniform response of the red channel within the scanning process [29]. The use of a single calibration curve for the entire range between 1.7 Gy and 42.5 Gy also introduces uncertainties in the order of 0.2 Gy from the calibration process alone. However, since all detectors were in good agreement within their measurement uncertainties, a reliable dosimetric characterization can be assumed. We plan to use the FD for future quality assurance of our FLASH beam.

In many countries, any LINAC operation requires a special license from a government agency tailored to the specifications of the equipment and its application. Therefore, any conversion of a licensed LINAC may require an extension of that license to include UHDR. In our case, all national regulations that standard LINACs have to comply with had to be fulfilled (e.g. the German Radiation Protection Act § 12, derived from the European Union Council Directive 2013/59/EURATOM), which implied an application for an extended license for UHDR research applications. In this context, an officially appointed expert (Section 181 of the German Radiation Protection Ordinance) had to approve UHDR before the first dose was administered. A relevant aspect of structural radiation protection [30] arises for UHDR if occupancy factors other than 1 were used for the design of the LINAC vault, since the maximum permissible weekly doses can be reached after a few minutes of beam-on time. In addition, the frequently required emergency stop buttons in LINAC vaults are of limited use due to the ultra-short dose delivery times. Full control of vault access and complete video surveillance of the treatment room should be ensured at all times.

Based on our experience, no increased radiation damage to the LINAC was detected at any time and quality control by certified medical physics experts after the LINAC was converted back to standard mode did not reveal any changes in LINAC behavior. This experience is in agreement with the observations of Sloop et al. [18] on a Varian LINAC. However, an analysis of a possible increased long-term degradation of LINAC components due to FLASH is beyond the scope of this work. Due to the fact that the LINAC was operated with the usual photon beam settings prior to the target and that the total dose was not increased, but only the DPP, this seems plausible. Most likely, even the disconnection of the ionization chamber was merely a precautionary measure [13,28].

Nevertheless, this work presents an efficient, fully reversible approach for the rapid conversion of an Elekta LINAC to FLASH mode and back. However, the authors neither claim generalizability of their approach to other similar devices, nor do they make any recommendations regarding the safety of the device itself and patient treatments after conversion. Finally, the LINAC vendor explicitly states that any potential harm from in-house modifications to the device is not part of any service contract, nor are any potential adverse consequences to routine patient treatments within their responsibility.

5. Conclusion

This study demonstrates the feasibility of converting a clinical LINAC to FLASH mode within 30 min. Neither permanent hardware modifications influencing the clinical beamline nor permanent software modifications influencing the clinical beam energy settings used for patient treatment are required. Maximum doses per pulse at SSD = 56 cm were 1.69 Gy with a dose rate of 676 Gy/s.

Declaration of competing interest

The authors declare that they have no known competing financial interests or personal relationships that could have appeared to influence the work reported in this paper.

Acknowledgements

The authors would like to thank Uwe Gros and Uwe Schröder from Elekta AB for their technical support on the LINAC's operating principle. We furthermore would like to thank Marcos Feijoo from BluePhysics for his support with the scintillation detector.

References

[1] Beddok A, Lahaye C, Calugaru V, De Marzi L, Fouillade C, Salvador S, et al. A comprehensive analysis of the relationship between dose rate and biological effects in preclinical and clinical studies, from brachytherapy to flattening filter free radiation therapy and FLASH irradiation. Int. J. Radiat. Oncol. Biol. Phys. 2022;113:985–95.
[2] Schuler E, Acharya M, Montay-Gruel P, Loo Jr BW, Vozenin MC, Maxim PG. Ultra-high dose rate electron beams and the FLASH effect: from preclinical evidence to a new radiotherapy paradigm. Med. Phys. 2022;49:2082–95.
[3] Chaikh A, Edouard M, Huet C, Milliat F, Villagrasa C, Isambert A. Towards clinical application of ultra-high dose rate radiotherapy and the FLASH effect: challenges and current status. Cancer Radiother. 2024;28:463–73.
[4] Esplen N, Mendonca MS, Bazalova-Carter M. Physics and biology of ultrahigh dose-rate (FLASH) radiotherapy: a topical review. Phys. Med. Biol. 2020;65:23TR03.
[5] Whitmore L, Mackay RI, van Herk M, Jones JK, Jones RM. Focused VHEE (very high energy electron) beams and dose delivery for radiotherapy applications. Sci. Rep. 2021;11:14013.
[6] Liu F, Shi J, Zha H, Li G, Li A, Gu W, et al. Development of a compact linear accelerator to generate ultrahigh dose rate high-energy X-rays for FLASH radiotherapy applications. Med. Phys. 2023;50:1680–98.
[7] Diffenderfer ES, Verginadis II, Kim MM, Shoniyozov K, Velalopoulou A, Goia D, et al. Design, Implementation, and in Vivo Validation of a Novel Proton FLASH Radiation Therapy System. Int. J. Radiat. Oncol. Biol. Phys. 2020;106:440–8.
[8] Diffenderfer ES, Sorensen BS, Mazal A, Carlson DJ. The current status of preclinical proton FLASH radiation and future directions. Med. Phys. 2022;49:2039–54.
[9] Tinganelli W, Sokol O, Quartieri M, Puspitasari A, Dokic I, Abdollahi A, et al. Ultra-High Dose Rate (FLASH) Carbon Ion Irradiation: Dosimetry and first Cell Experiments. Int. J. Radiat. Oncol. Biol. Phys. 2022;112:1012–22.
[10] Xie DH, Li YC, Ma S, Yang X, Lan RM, Chen AQ, et al. Electron ultra-high dose rate FLASH irradiation study using a clinical linac: linac modification, dosimetry, and radiobiological outcome. Med. Phys. 2022;49:6728–38.
[11] Dal Bello R, von der Grun J, Fabiano S, Rudolf T, Saltybaeva N, Stark LS, et al. Enabling ultra-high dose rate electron beams at a clinical linear accelerator for isocentric treatments. Radiother. Oncol. 2023;187:109822.
[12] Schuler E, Trovati S, King G, Lartey F, Rafat M, Villegas M, et al. Experimental platform for ultra-high dose rate FLASH irradiation of small animals using a clinical linear accelerator. Int. J. Radiat. Oncol. Biol. Phys. 2017;97:195–203.
[13] Konradsson E, Wahlqvist P, Thoft A, Blad B, Back S, Ceberg C, et al. Beam control system and output fine-tuning for safe and precise delivery of FLASH radiotherapy at a clinical linear accelerator. Front. Oncol. 2024;14:1342488.
[14] Lempart M, Blad B, Adrian G, Back S, Knoos T, Ceberg C, et al. Modifying a clinical linear accelerator for delivery of ultra-high dose rate irradiation. Radiother. Oncol. 2019;139:40–5.

[15] No HJ, Wu YF, Dworkin ML, Manjappa R, Skinner L, Ashraf MR, et al. Clinical linear accelerator-based electron FLASH: pathway for practical translation to FLASH clinical trials. Int. J. Radiat. Oncol. Biol. Phys. 2023;117:482–92.
[16] Rahman M, Ashraf MR, Zhang R, Bruza P, Dexter CA, Thompson L, et al. Electron FLASH delivery at treatment room isocenter for efficient reversible conversion of a clinical LINAC. Int. J. Radiat. Oncol. Biol. Phys. 2021;110:872–82.
[17] Cetnar AJ, Jain S, Gupta N, Chakravarti A. Technical note: commissioning of a linear accelerator producing ultra-high dose rate electrons. Med. Phys. 2024;51:1415–20.
[18] Sloop A, Ashraf MR, Rahman M, Sunnerberg J, Dexter CA, Thompson L, et al. Rapid switching of a C-series linear accelerator between conventional and ultrahigh-dose-rate research mode with beamline modifications and output stabilization. Int. J. Radiat. Oncol. Biol. Phys. 2024;119:1317–25.
[19] Deut UCA, Cavicchi C, Cirio R, Data EM, Durisi EA, Ferrero V, Ferro A, Giordanengo S, Villarreal OM, et al. Clinical linear accelerator for ultra-high dose rate beam delivery. Appl. Sci. 2024;14:1–14.
[20] Das IJ, Sohn JJ, Lim SN, Sengupta B, Feijoo M, Yadav P. Characteristics of a plastic scintillation detector in photon beam dosimetry. J. Appl. Clin. Med. Phys. 2024;25:e14209.
[21] Palmiero A, Liu K, Colnot J, Chopra N, Neill D, Connell L, et al. On the acceptance, commissioning, and quality assurance of electron FLASH units. Med. Phys. 2025;52:1207–23.
[22] Marinelli M, Felici G, Galante F, Gasparini A, Giuliano L, Heinrich S, et al. Design, realization, and characterization of a novel diamond detector prototype for FLASH radiotherapy dosimetry. Med. Phys. 2022;49:1902–10.
[23] Verona Rinati G, Felici G, Galante F, Gasparini A, Kranzer R, Mariani G, et al. Application of a novel diamond detector for commissioning of FLASH radiotherapy electron beams. Med. Phys. 2022;49:5513–22.
[24] Petersson K, Jaccard M, Germond JF, Buchillier T, Bochud F, Bourhis J, et al. High dose-per-pulse electron beam dosimetry - a model to correct for the ion recombination in the Advanced Markus ionization chamber. Med. Phys. 2017;44:1157–67.
[25] Liu K, Holmes S, Schuler E, Beddar S. A comprehensive investigation of the performance of a commercial scintillator system for applications in electron FLASH radiotherapy. Med. Phys. 2024;51:4504–12.
[26] Karsch L, Beyreuther E, Burris-Mog T, Kraft S, Richter C, Zeil K, et al. Dose rate dependence for different dosimeters and detectors: TLD, OSL, EBT films, and diamond detectors. Med. Phys. 2012;39:2447–55.
[27] Jaccard M, Petersson K, Buchillier T, Germond JF, Duran MT, Vozenin MC, et al. High dose-per-pulse electron beam dosimetry: Usability and dose-rate independence of EBT3 Gafchromic films. Med. Phys. 2017;44:725–35.
[28] Szpala S, Huang V, Zhao Y, Kyle A, Minchinton A, Karan T, et al. Dosimetry with a clinical linac adapted to FLASH electron beams. J. Appl. Clin. Med. Phys. 2021;22:50–9.
[29] Shameem T, Bennie N, Butson M, Thwaites D. Effect of scanner lens on lateral response artefact in radiochromic film dosimetry. Phys. Eng. Sci. Med. 2022;45:721–7.
[30] Praestegaard LH. Radiation safety of ultra-high dose rate electron accelerators for FLASH radiotherapy. Med. Phys. 2024;51:6206–19.